ELSEVIER

Physics Letters B 526 (2002) 34–49

PHYSICS LETTERS B

www.elsevier.com/locate/npe

Production of D_s^{**} mesons in hadronic Z decays

ALEPH Collaboration

A. Heister, S. Schael

Physikalisches Institut das RWTH-Aachen, D-52056 Aachen, Germany

R. Barate, I. De Bonis, D. Decamp, C. Goy, J.-P. Lees, E. Merle, M.-N. Minard, B. Pietrzyk

Laboratoire de Physique des Particules (LAPP), IN^2P^3-CNRS, F-74019 Annecy-le-Vieux Cedex, France

G. Boix, S. Bravo, M.P. Casado, M. Chmeissani, J.M. Crespo, E. Fernandez, M. Fernandez-Bosman, Ll. Garrido [15], E. Graugés, M. Martinez, G. Merino, R. Miquel [27], Ll.M. Mir [27], A. Pacheco, H. Ruiz

Institut de Física d'Altes Energies, Universitat Autònoma de Barcelona, E-08193 Bellaterra, Barcelona, Spain [7]

A. Colaleo, D. Creanza, M. de Palma, G. Iaselli, G. Maggi, M. Maggi, S. Nuzzo, A. Ranieri, G. Raso [23], F. Ruggieri, G. Selvaggi, L. Silvestris, P. Tempesta, A. Tricomi [3], G. Zito

Dipartimento di Fisica, INFN Sezione di Bari, I-70126 Bari, Italy

X. Huang, J. Lin, Q. Ouyang, T. Wang, Y. Xie, R. Xu, S. Xue, J. Zhang, L. Zhang, W. Zhao

Institute of High Energy Physics, Academia Sinica, Beijing, People's Republic of China [8]

D. Abbaneo, P. Azzurri, O. Buchmüller [25], M. Cattaneo, F. Cerutti, B. Clerbaux, H. Drevermann, R.W. Forty, M. Frank, F. Gianotti, T.C. Greening [29], J.B. Hansen, J. Harvey, D.E. Hutchcroft, P. Janot, B. Jost, M. Kado [27], P. Mato, A. Moutoussi, F. Ranjard, L. Rolandi, D. Schlatter, O. Schneider [2], G. Sguazzoni, W. Tejessy, F. Teubert, A. Valassi, I. Videau, J. Ward

European Laboratory for Particle Physics (CERN), CH-1211 Geneva 23, Switzerland

PII: S0370-2693(01)01465-4

F. Badaud, A. Falvard [22], P. Gay, P. Henrard, J. Jousset, B. Michel, S. Monteil, J.-C. Montret, D. Pallin, P. Perret

Laboratoire de Physique Corpusculaire, Université Blaise Pascal, IN^{2}P^3-CNRS, Clermont-Ferrand, F-63177 Aubière, France

J.D. Hansen, J.R. Hansen, P.H. Hansen, B.S. Nilsson, A. Wäänänen

Niels Bohr Institute, DK-2100 Copenhagen, Denmark [9]

A. Kyriakis, C. Markou, E. Simopoulou, A. Vayaki, K. Zachariadou

Nuclear Research Center Demokritos (NRCD), GR-15310 Attiki, Greece

A. Blondel [12], G. Bonneaud, J.-C. Brient, A. Rougé, M. Rumpf, M. Swynghedauw, M. Verderi, H. Videau

Laboratoire de Physique Nucléaire et des Hautes Energies, Ecole Polytechnique, IN^{2}P^3-CNRS, F-91128 Palaiseau Cedex, France

V. Ciulli, E. Focardi, G. Parrini

Dipartimento di Fisica, Università di Firenze, INFN Sezione di Firenze, I-50125 Firenze, Italy

A. Antonelli, M. Antonelli, G. Bencivenni, G. Bologna [4], F. Bossi, P. Campana, G. Capon, V. Chiarella, P. Laurelli, G. Mannocchi [5], F. Murtas, G.P. Murtas, L. Passalacqua, M. Pepe-Altarelli [24], P. Spagnolo

Laboratori Nazionali dell'INFN (LNF-INFN), I-00044 Frascati, Italy

A. Halley, J.G. Lynch, P. Negus, V. O'Shea, C. Raine [4], A.S. Thompson

Department of Physics and Astronomy, University of Glasgow, Glasgow G12 8QQ, UK [10]

S. Wasserbaech

Department of Physics, Haverford College, Haverford, PA 19041-1392, USA

R. Cavanaugh, S. Dhamotharan, C. Geweniger, P. Hanke, G. Hansper, V. Hepp, E.E. Kluge, A. Putzer, J. Sommer, K. Tittel, S. Werner [19], M. Wunsch [19]

Kirchhoff-Institut für Physik, Universität Heidelberg, D-69120 Heidelberg, Germany [16]

R. Beuselinck, D.M. Binnie, W. Cameron, P.J. Dornan, M. Girone [1], N. Marinelli, J.K. Sedgbeer, J.C. Thompson [14]

Department of Physics, Imperial College, London SW7 2BZ, UK [10]

V.M. Ghete, P. Girtler, E. Kneringer, D. Kuhn, G. Rudolph

Institut für Experimentalphysik, Universität Innsbruck, A-6020 Innsbruck, Austria [18]

E. Bouhova-Thacker, C.K. Bowdery, A.J. Finch, F. Foster, G. Hughes, R.W.L. Jones, M.R. Pearson, N.A. Robertson

Department of Physics, University of Lancaster, Lancaster LA1 4YB, UK [10]

K. Jakobs, K. Kleinknecht, G. Quast [6], B. Renk, H.-G. Sander, H. Wachsmuth, C. Zeitnitz

Institut für Physik, Universität Mainz, D-55099 Mainz, Germany [16]

A. Bonissent, J. Carr, P. Coyle, O. Leroy, P. Payre, D. Rousseau, M. Talby

Centre de Physique des Particules, Université de la Méditerranée, IN^{2}P^3-CNRS, F-13288 Marseille, France

F. Ragusa

Dipartimento di Fisica, Università di Milano e INFN Sezione di Milano, I-20133 Milano, Italy

A. David, H. Dietl, G. Ganis [26], K. Hüttmann, G. Lütjens, C. Mannert, W. Männer, H.-G. Moser, R. Settles, H. Stenzel, W. Wiedenmann, G. Wolf

Max-Planck-Institut für Physik, Werner-Heisenberg-Institut, D-80805 München, Germany [16]

J. Boucrot, O. Callot, M. Davier, L. Duflot, J.-F. Grivaz, Ph. Heusse, A. Jacholkowska [22], J. Lefrançois, J.-J. Veillet, C. Yuan

Laboratoire de l'Accélérateur Linéaire, Université de Paris-Sud, IN^{2}P^3-CNRS, F-91898 Orsay Cedex, France

G. Bagliesi, T. Boccali, L. Foà, A. Giammanco, A. Giassi, F. Ligabue, A. Messineo, F. Palla, G. Sanguinetti, A. Sciabà, R. Tenchini [1], A. Venturi [1], P.G. Verdini

Dipartimento di Fisica dell'Università, INFN Sezione di Pisa, e Scuola Normale Superiore, I-56010 Pisa, Italy

G.A. Blair, G. Cowan, M.G. Green, T. Medcalf, A. Misiejuk, J.A. Strong, P. Teixeira-Dias, J.H. von Wimmersperg-Toeller

Department of Physics, Royal Holloway & Bedford New College, University of London, Egham, Surrey TW20 OEX, UK [10]

R.W. Clifft, T.R. Edgecock, P.R. Norton, I.R. Tomalin

Particle Physics Dept., Rutherford Appleton Laboratory, Chilton, Didcot, Oxon OX11 OQX, UK [10]

B. Bloch-Devaux [1], P. Colas, S. Emery, W. Kozanecki, E. Lançon, M.-C. Lemaire, E. Locci, P. Perez, J. Rander, J.-F. Renardy, A. Roussarie, J.-P. Schuller, J. Schwindling, A. Trabelsi [21], B. Vallage

CEA, DAPNIA/Service de Physique des Particules, CE-Saclay, F-91191 Gif-sur-Yvette Cedex, France [17]

N. Konstantinidis, A.M. Litke, G. Taylor

Institute for Particle Physics, University of California at Santa Cruz, Santa Cruz, CA 95064, USA [13]

C.N. Booth, S. Cartwright, F. Combley [4], M. Lehto, L.F. Thompson

Department of Physics, University of Sheffield, Sheffield S3 7RH, UK [10]

K. Affholderbach [28], A. Böhrer, S. Brandt, C. Grupen, A. Ngac, G. Prange, U. Sieler

Fachbereich Physik, Universität Siegen, D-57068 Siegen, Germany [16]

G. Giannini

Dipartimento di Fisica, Università di Trieste e INFN Sezione di Trieste, I-34127 Trieste, Italy

J. Rothberg

Experimental Elementary Particle Physics, University of Washington, Seattle, WA 98195, USA

S.R. Armstrong, K. Berkelman, K. Cranmer, D.P.S. Ferguson, Y. Gao [20], S. González, O.J. Hayes, H. Hu, S. Jin, J. Kile, P.A. McNamara III, J. Nielsen, Y.B. Pan, J.H. von Wimmersperg-Toeller, W. Wiedenmann, J. Wu, Sau Lan Wu, X. Wu, G. Zobernig

Department of Physics, University of Wisconsin, Madison, WI 53706, USA [11]

G. Dissertori

Institute for Particle Physics, ETH Hönggerberg, HPK, 8093 Zürich, Switzerland

Received 29 November 2001; accepted 12 December 2001
Editor: L. Montanet

Abstract

The production rates of the orbitally excited D_s^{**} mesons, $D_{s1}^{\pm}$ and $D_{s2}^{*\pm}$, are measured with the 4.1 million hadronic Z decays recorded by the ALEPH detector during 1991–1995. The D_s^{**} mesons are reconstructed in the decay modes $D_{s1}^{+} \to D^{*+}K^0$, $D_{s1}^{+} \to D^{*0}K^+$ and $D_{s2}^{*+} \to D^0K^+$. The production rate of the $D_{s1}^{\pm}$ is measured to be $f(Z \to D_{s1}^{\pm}) = (0.52 \pm 0.09 \pm 0.06)\%$, under the assumption that the two considered decay modes of the $D_{s1}^{\pm}$ saturate the branching ratio. The production rate of the $D_{s2}^{*\pm}$ is determined to be $f(Z \to D_{s2}^{*\pm}) = (0.83 \pm 0.29^{+0.07}_{-0.13})\%$, assuming that the branching fraction of the decay $D_{s2}^{*+} \to D^0K^+$ is 45%. The production rates in $Z \to c\bar{c}$ and $Z \to b\bar{b}$ decays are measured separately.

E-mail address: christian.zeitnitz@uni-mainz.de (C. Zeitnitz).
[1] Also at CERN, 1211 Geneva 23, Switzerland.
[2] Now at Université de Lausanne, 1015 Lausanne, Switzerland.
[3] Also at Dipartimento di Fisica di Catania and INFN Sezione di Catania, 95129 Catania, Italy.
[4] Deceased.
[5] Also Istituto di Cosmo-Geofisica del C.N.R., Torino, Italy.
[6] Now at Institut für Experimentelle Kernphysik, Universität Karlsruhe, 76128 Karlsruhe, Germany.
[7] Supported by CICYT, Spain.
[8] Supported by the National Science Foundation of China.
[9] Supported by the Danish Natural Science Research Council.
[10] Supported by the UK Particle Physics and Astronomy Research Council.
[11] Supported by the US Department of Energy, grant DE-FG0295-ER40896.
[12] Now at Departement de Physique Corpusculaire, Université de Genève, 1211 Genève 4, Switzerland.
[13] Supported by the US Department of Energy, grant DE-FG03-92ER40689.
[14] Also at Rutherford Appleton Laboratory, Chilton, Didcot, UK.
[15] Permanent address: Universitat de Barcelona, 08208 Barcelona, Spain.
[16] Supported by the Bundesministerium für Bildung, Wissenschaft, Forschung und Technologie, Germany.
[17] Supported by the Direction des Sciences de la Matière, CEA.
[18] Supported by the Austrian Ministry for Science and Transport.
[19] Now at SAP AG, 69185 Walldorf, Germany.
[20] Also at Department of Physics, Tsinghua University, Beijing, People's Republic of China.
[21] Now at Département de Physique, Faculté des Sciences de Tunis, 1060 Le Belvédère, Tunisia.
[22] Now at Groupe d' Astroparticules de Montpellier, Université de Montpellier II, 34095 Montpellier, France.
[23] Also at Dipartimento di Fisica e Tecnologie Relative, Università di Palermo, Palermo, Italy.
[24] Now at CERN, 1211 Geneva 23, Switzerland.
[25] Now at SLAC, Stanford, CA 94309, USA.
[26] Now at INFN Sezione di Roma II, Dipartimento di Fisica, Universitá di Roma Tor Vergata, 00133 Roma, Italy.
[27] Now at LBNL, Berkeley, CA 94720, USA.
[28] Now at Skyguide, Swissair Navigation Services, Geneva, Switzerland.
[29] Now at Honeywell, Phoenix, AZ, USA.

1. Introduction

Four orbitally-excited D_s^{**} mesons, with angular momentum $L = 1$, are expected to exist in addition to the pseudoscalar and vector mesons D_s and D_s^*. In the Heavy Quark Effective Theory [1,2] the spin of the light quark couples with the orbital angular momentum to give $j = 1/2$ or $j = 3/2$. When coupled to the spin of the heavy quark, two doublets are obtained with the quantum numbers $J^P = 0^+, 1^+$ and $J^P = 1^+, 2^+$, respectively. These states are expected to decay mainly into DK or D*K modes.

Only certain S- and D-wave decays are allowed by spin and parity conservation. The states of the $(j = 1/2)$ doublet decay via S-wave transitions and are therefore expected to be broad ($\Gamma > 100$ MeV); they have not been observed yet. The $(j = 3/2)$ doublet states are much narrower since they can only decay via D-wave modes. The two narrow states[30] $D_{s1}^{\pm}$ and $D_{s2}^{*\pm}$ have been observed by ARGUS and CLEO [3–5]. At LEP, $D_{s1}^{\pm}$ mesons have been observed by OPAL [6]. The properties of the four D_s^{**} states are listed in Table 1. The actual physical particles could be superpositions of the individual states.

In this analysis the production rates of the two narrow states are measured in the decay modes[31] $D_{s1}^+ \to D^{*+}K^0$, $D_{s1}^+ \to D^{*0}K^+$ and $D_{s2}^{*+} \to D^0K^+$. In $Z \to c\bar{c}$ events, D_s^{**} mesons are produced in the fragmentation of primary c-quarks, whereas in $Z \to b\bar{b}$ events they can only be produced in decays of b hadrons. To study these two contributions separately, b- and c-quark-enriched event samples are also used.

2. The ALEPH detector

The ALEPH detector and its performance are described in detail elsewhere [9,10]. Only a brief overview of the apparatus is given here. Surrounding the beam pipe, a high resolution vertex detector (VDET) consists of two layers of double-sided silicon microstrip detectors, positioned at average radii of 6.5 cm and 11.3 cm, and covering, respectively, 85% and 69% of the solid angle. The spatial resolution for the $r\phi$ and z projections (transverse to and along the beam axis, respectively) is 12 μm at normal incidence. The vertex detector is surrounded by a drift chamber with eight coaxial wire layers with an outer radius of 26 cm and by a time projection chamber (TPC) that measures up to 21 three-dimensional points per track at radii between 30 cm and 180 cm. These detectors are immersed in an axial magnetic field of 1.5 T provided by a superconducting solenoidal coil and together measure the transverse momenta of charged particles with a resolution $\sigma(p_T)/p_T = 6 \times 10^{-4} p_T \oplus 0.005$ (p_T in GeV/c). The resolution of the three-dimensional impact parameter for tracks having information from all tracking detectors and two VDET hits (a VDET "hit" being defined as a space point reconstructed from the $r\phi$ and z coordinates) can be parametrized as $\sigma = 25\ \mu m + 95\ \mu m/p$ (p in GeV/c). The TPC also provides up to 338 measurements of the specific ionization of a charged particle. The TPC is surrounded by a lead/proportional-chamber electromagnetic calorimeter segmented into $0.9^\circ \times 0.9^\circ$ projective towers and read out in three sections in depth, with energy resolution $\sigma(E)/E = 0.18/\sqrt{E} + 0.009$ (E in GeV). The iron return yoke of the magnet is instrumented with streamer tubes to form a hadron calorimeter, with a thickness of over 7 interaction lengths, and is surrounded by two layers of muon chambers. An algorithm combines all these measurements to provide a determination of the energy flow [10] with an uncertainty on the measurable total energy of $\sigma(E) = (0.6\sqrt{E/\text{GeV}} + 0.6)$ GeV.

2.1. Event and track selection

This analysis uses 4.1 million hadronic events recorded by the ALEPH detector at centre-of-mass energies close to the Z mass. The events are selected with the charged particle requirements described in [11]. The helix fit of the charged particle tracks used for the D_s^{**} reconstruction must have a χ^2 per degree of freedom smaller than 5, and their polar angle must satisfy $|\cos\theta| < 0.95$. Finally, the distance to the primary vertex in the plane transverse to the beam axis has to be less than 2 cm and in the beam direction less than 10 cm.

[30] The notation used follows that of the Particle Data Group [7] for the D** mesons.

[31] Throughout this Letter the notation used for particles implies the charge-conjugate modes as well.

Table 1
Masses and decay modes of D_s^{**} mesons

	J^P	D^0K^+	D^+K^0	$D^{*0}K^+$	$D^{*+}K^0$	Mass [MeV/c^2]	Width [MeV]
D_{s1}^+	1^+	×	×	D-wave	D-wave	2535.3 ± 0.6 [7]	< 2.3 (95% CL) [7]
D_{s0}^{*+}	0^+	S-wave	S-wave	×	×	–	> 100 [8]
D_{s1}^{*+}	1^+	×	×	S-wave	S-wave	–	> 100 [8]
D_{s2}^{*+}	2^+	D-wave	D-wave	D-wave	D-wave	2573.5 ± 1.7 [7]	15^{+5}_{-4} [7]

2.2. Particle identification

Charged kaons are identified by means of the specific ionization loss dE/dx in the TPC. The TPC provides two different measurements of the deposited energy, from the wire and the pad readout. The wire readout is only used if at least 50 individual wire samples are available. In this case the pad readout is ignored. If the wire information is insufficient the pad readout is exploited. In both cases the particle identification is based on the dE/dx estimator r_π (r_K), defined as the difference between the expected and the measured ionization loss expressed in terms of standard deviations for the pion (kaon) mass hypothesis. A track is accepted as a kaon if its momentum is greater than 1.5 GeV/c, $|r_K|$ is less than 2.5 and it satisfies $r_K + r_\pi < 0$.

Neutral kaons are reconstructed in the decay mode $K_S^0 \to \pi^+\pi^-$ as described in [12]. For the identification of the K_S^0 their long lifetime ($c\tau = 2.7$ cm) is exploited by only accepting neutral vertices with a distance of at least 1.5 cm to the primary vertex and a $\chi^2 < 13$ of the vertex fit. The reconstructed mass of the K_S^0 candidate has to be within 12 MeV/c^2 of the nominal K_S^0 mass.

Charged pions are selected by requiring $|r_\pi|$ to be smaller than 2.5. Neutral pions are reconstructed by a mass-constrained fit to the detected photons in the electromagnetic calorimeter [10]. The momentum of the π^0 candidate has to be greater than 1.5 GeV/c and the χ^2 of the mass fit less than 8.

2.3. Selection of c- and b-quark-enriched event samples

To determine the production rates of D_s^{**} in $Z \to c\bar{c}$ and $Z \to b\bar{b}$ events separately, c- and b-quark-enriched event samples have been selected. Due to the good spatial resolution of the vertex detector, the probability ($\mathcal{P}_{evt}$) that all charged tracks originate from the primary vertex, determined with the algorithm described in [13], can be used to separate long-lived b-hadrons (low probability $\mathcal{P}_{evt}$) from c- and uds-events.

Table 2
Cuts for the selection of the c- and b-quark-enriched event sample

c-quark-enriched sample	b-quark-enriched sample
0.1 ps $< t <$ 1.5 ps	$t >$ 0.4 ps
$-\log_{10}(\mathcal{P}_{evt}) < 4$	$-\log_{10}(\mathcal{P}_{evt}) > 1.5$
$x_E > 0.4$	$0.25 < x_E < 0.65$

An additional separation between c- and b-events is obtained by a cut on the scaled energy x_E (normalized to the beam energy) of the D_s^{**} candidate, because less energy is available for c quarks originating from a b-hadron decay than in direct $Z \to c\bar{c}$ decays.

A D^0 is reconstructed in all the decay modes considered. In order to further separate light (uds) from heavy (c and b) quark events, a cut on the proper decay time of the D^0 candidate is performed. The proper decay time is determined from the decay length l, calculated as the distance of the D^0 decay vertex from the primary vertex, projected along the momentum vector of the D^0, and taking $t = M_{D^0} \cdot l/p$.

The cuts used to select the enriched samples are listed in Table 2. About 4% of all events are rejected because they pass the cuts for the c- as well as the b-quark selection.

3. Reconstruction of D_{s1}^+ and D_{s2}^{*+}

3.1. Decay channel $D_{s1}^+ \to D^{*+}K^0$

The D^{*+} mesons are reconstructed in the decay channel $D^{*+} \to D^0\pi^+$ and D^0 mesons in the four decay channels $D^0 \to K^-\pi^+$, $D^0 \to \overline{K}^0\pi^+\pi^-$, $D^0 \to$

Table 3
Cuts for the reconstruction of D^0 mesons in the decay channels $D^0 \to K^-\pi^+$, $D^0 \to \overline{K}^0\pi^+\pi^-$, $D^0 \to K^-\pi^+\pi^-\pi^+$ and $D^0 \to K^-\pi^+\pi^0$

Variable	Decay channel			
	$D^0 \to K^-\pi^+$	$D^0 \to \overline{K}^0\pi^+\pi^-$	$D^0 \to K^-\pi^+\pi^-\pi^+$	$D^0 \to K^-\pi^+\pi^0$
ΔM_{D^0}	± 20 MeV/c^2	± 20 MeV/c^2	± 15 MeV/c^2	± 25 MeV/c^2
p_K	> 1.5 GeV/c	> 3.0 GeV/c	> 2.0 GeV/c	> 2.0 GeV/c
p_π	> 0.7 GeV/c	> 1.0 GeV/c	> 0.4 GeV/c	> 2.0 GeV/c
p_π (2nd)	–	> 1.0 GeV/c	> 1.5 GeV/c	–
p_π (3rd)	–	–	> 2.0 GeV/c	–

$K^-\pi^+\pi^-\pi^+$ and $D^0 \to K^-\pi^+\pi^0$. Because the combinatorial background is suppressed by the good resolution on the mass-difference between the D^{*+} and D^0 meson, the cuts for the selection of D^0 mesons are rather loose.

To avoid double counting in the D^0 decay channels with charged kaons and pions, the track with the smallest value of r_K is assumed to be the kaon track. A fit to a common decay vertex is performed for the tracks of the selected charged particles and the χ^2 has to be less than 20. The momentum of the D^0 candidate has to be greater than 7 GeV/c. Additional cuts are listed in Table 3. The selected D^0 candidates are combined with all charged pions with a momentum less than 3 GeV/c. For the D^{*+} candidates with a momentum greater than 8 GeV/c, the mass difference $\Delta M_1 = m(D^0, \pi^+) - m(D^0)$ is calculated. The ΔM_1 distributions for the four D^0 decay channels are shown in Fig. 1. The number of reconstructed D^{*+} mesons is determined by a fit to the measured ΔM_1 distributions. The signal is parametrized as a Breit–Wigner and the background shape with the following function:

$$\frac{dN}{d(\Delta M)} \propto (\Delta M - a)^b e^{-c(\Delta M - a)}.$$

Each D^{*+} candidate inside the signal region (± 1.5 MeV/c^2) is combined with all K^0_S candidates with a momentum greater than 2.5 GeV/c. The combination of the D^{*+} and the K^0_S is required to have a scaled energy x_E greater than 0.25. The mass difference $\Delta M_2 = m(D^{*+}, K^0) - m(D^{*+}) - m(K^0) + m_{\text{true}}(K^0)$ is calculated, where $m_{\text{true}}(K^0)$ is the nominal K^0 mass, because this quantity has the best resolution. The resulting mass difference distribution ΔM_2 is shown in Fig. 2(a). The distribution shows an excess of events in the signal region around 525 MeV/c^2. The combinatorial background (Fig. 2(b)) is determined with the help of D^{*+} candidates from sidebands above the D^{*+} mass window (Fig. 1). The number of signal events and the mass difference ΔM_2 are determined by a simultaneous unbinned log-likelihood fit to the signal and background distributions, with the decay width of the D^+_{s1} fixed to 1.5 MeV. The signal is fitted with a Breit–Wigner function, convoluted with the detector resolution. The detector resolutions for the reconstruction of D^+_{s1} mesons in the different D^0 decay channels are determined from simulated events. The resolution is approximately 1.7 MeV/c^2 for the D^0 decay channels $D^0 \to K^-\pi^+$, $D^0 \to \overline{K}^0\pi^+\pi^-$ and $D^0 \to K^-\pi^+\pi^-\pi^+$ and 2.6 MeV/c^2 for the channel $D^0 \to K^-\pi^+\pi^0$.

Table 4
Results of the fits to the flavour-independent sample

Decay channel	No. of events	ΔM [MeV/c^2]
$D^+_{s1} \to D^{*+}K^0$	$40.9 \pm 8.4_{\text{stat}}{}^{+3.2}_{-3.7\,\text{syst}}$	$525.3 \pm 0.6_{\text{stat}} \pm 0.1_{\text{syst}}$
$D^+_{s1} \to D^{*0}K^+$	$51.3 \pm 13.9_{\text{stat}}{}^{+3.8}_{-4.0\,\text{syst}}$	$528.7 \pm 1.9_{\text{stat}} \pm 0.5_{\text{syst}}$
$D^{*+}_{s2} \to D^0K^+$	$63.6 \pm 21.9_{\text{stat}}{}^{+4.1}_{-9.5\,\text{syst}}$	$704 \pm 3_{\text{stat}} \pm 1_{\text{syst}}$

The results of the fit to the ΔM_2 distribution are listed in Table 4. The systematic errors on the mass differences are obtained by varying, in the fit, the assumed natural width of the D^+_{s1} meson and the detector resolution, as described in Section 5.1.

3.2. *Decay channels* $D^+_{s1} \to D^{*0}K^+$ *and* $D^{*+}_{s2} \to D^0K^+$

The D^{*0} mesons decay into a D^0 by emitting a π^0 or a photon. Because of the higher background in these channels the selection of D^0 candidates has to be more restrictive than for D^0 candidates used in the reconstruction of D^{*+} mesons. An acceptable signal-to-background ratio is only achieved in the decay channel $D^0 \to K^-\pi^+$ and therefore only this

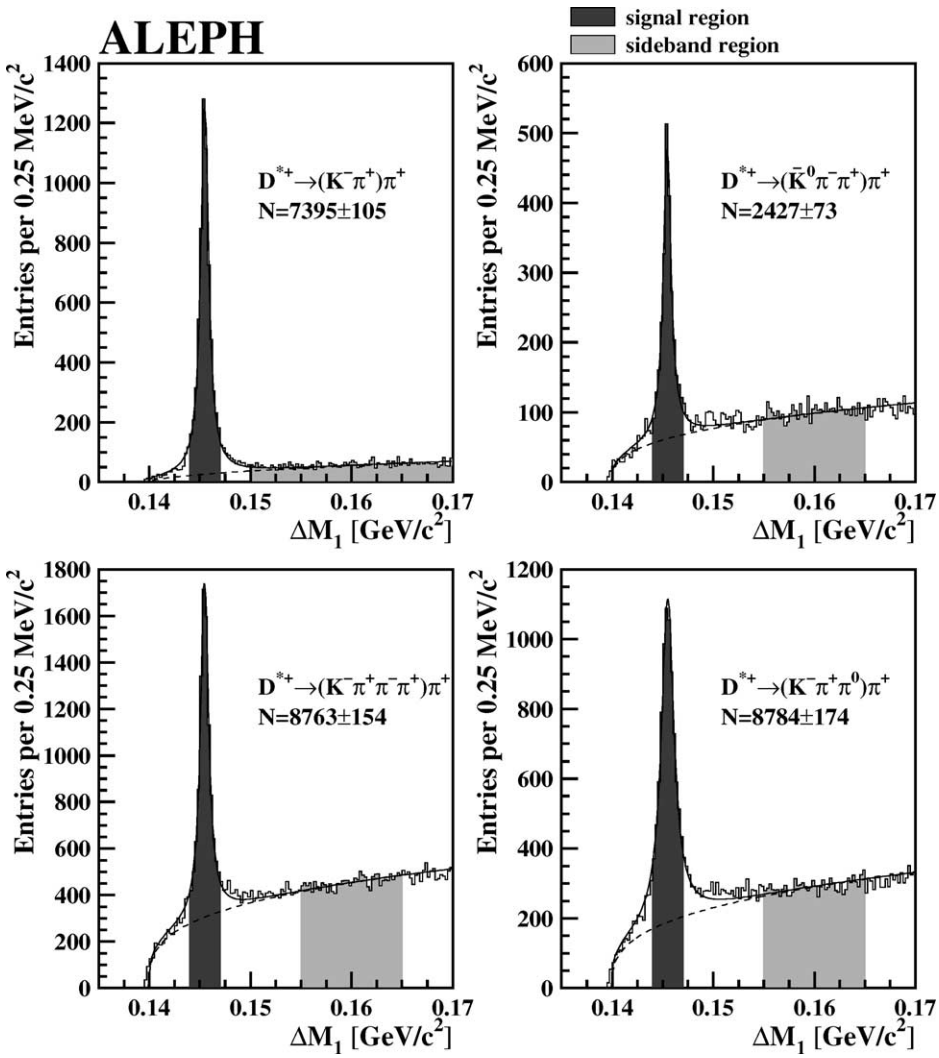

Fig. 1. Reconstructed mass-difference distribution of ΔM_1. The quoted numbers of D^{*+} candidates are obtained from a fit to the distribution.

channel was used for the analysis. The D^0 candidates are rejected if the invariant mass of the D^0 and any π^+ in the event is within 2 MeV/c^2 of the D^{*+} mass window. The cuts on the momentum of the D^0 candidate and on that of the decay particles are tightened to 8 GeV/c and 3 GeV/c, respectively. The D^0 candidate is also required to have a proper decay time greater than 0.2 ps. The latter cut removes combinatorial background, peaked at small proper time. The invariant mass distribution of the selected D^0 candidates is shown in Fig. 3. The π^0 or photon from the D^{*0} decay is not reconstructed in this analysis. Instead the combination of the D^0 with all charged kaons in the event with momentum greater than 3 GeV/c is taken and the mass difference $\Delta M_3 = m(D^0, K^+) - m(D^0)$ is calculated. Because of the small Q-value in the decay $D^{*0} \to D^0\pi^0$ of only 7 MeV, this procedure does not significantly change the resolution, which is determined from the simulation to be (2.9 ± 0.1) MeV/c^2. In the case where the D^{*0} emits a photon the resolution is (7.1 ± 0.2) MeV/c^2.

The D_{s2}^{*+} meson is allowed to decay directly into the D^0K^+ final state and therefore the mass difference

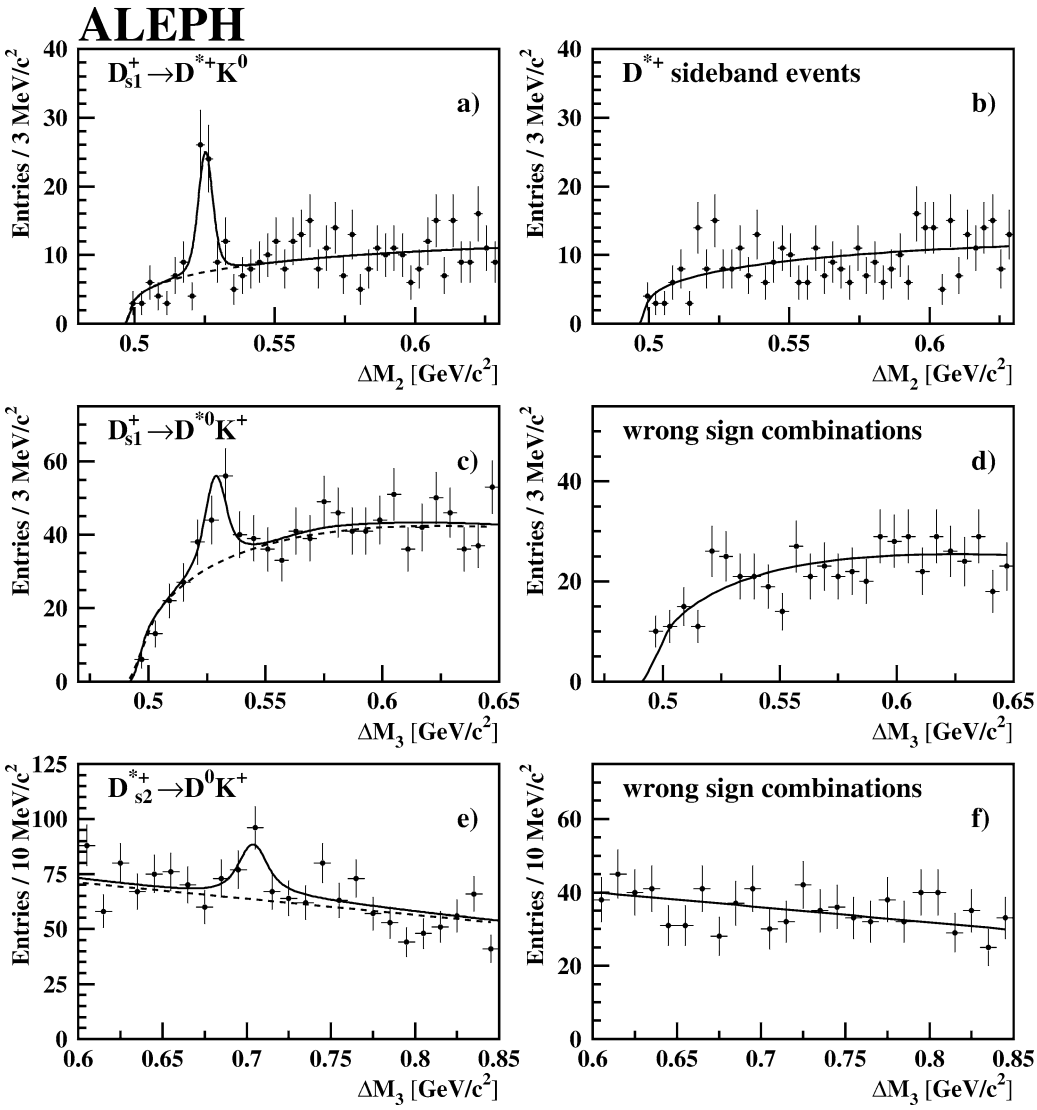

Fig. 2. Reconstructed mass-difference distribution for the decays $D_{s1}^+ \to D^{*+}K^0$ ((a) and (b)), $D_{s1}^+ \to D^{*0}K^+$ ((c) and (d)) and $D_{s2}^{*+} \to D^0K^+$ ((e) and (f)). The full curve is the result of an unbinned log-likelihood fit and the dashed curve represents the combinatorial background.

ΔM_3 is also used to measure the decay $D_{s2}^{*+} \to D^0K^+$. The detector resolution in the reconstruction of this decay is (3.1 ± 0.1) MeV/c^2. The decay $D_{s2}^{*+} \to D^{*0}K^+$ is also allowed but suppressed due to the smaller phase space.

The measured mass-difference distribution for D^0K^+ combinations with a scaled energy greater than 0.25 is shown in Figs. 2(c)–(f). Signals for the $D_{s1}^+ \to D^{*0}K^+$ (Fig. 2(c)) and $D_{s2}^{*+} \to D^0K^+$ decays (Fig. 2(e)) are visible, as expected, around 525 MeV/c^2 and 710 MeV/c^2, respectively. The shape of the combinatorial background is determined with the help of the wrong-sign charge combinations D^0K^- (Figs. 2(d) and (f)). The shape of the combinatorial background for the decay of the D_{s1}^+ is parameterized with the function given in Section 3.1. The combinatorial background for the decay of the D_{s2}^{*+} is described by a linear function of ΔM_3. The num-

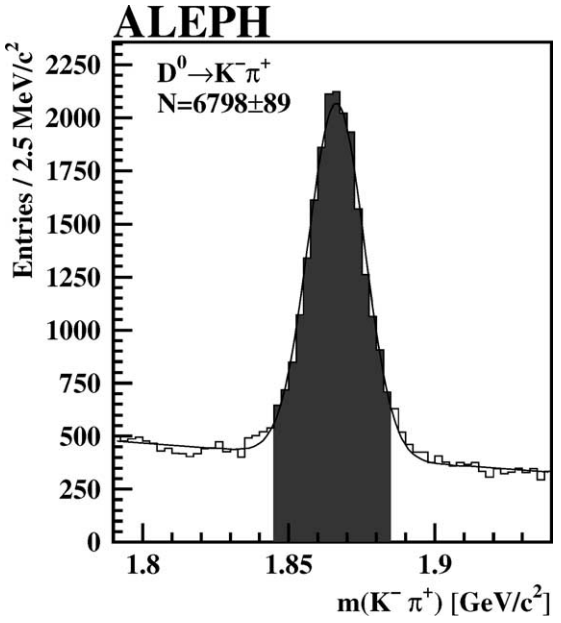

Fig. 3. Invariant mass of the $D^0 \to K^-\pi^+$ candidates. The events in the shaded region are used for the reconstruction of the $D_{s1}^+ \to D^{*0}K^+$ and $D_{s2}^{*+} \to D^0K^+$ decays.

bers of signal events are determined with a simultaneous unbinned log-likelihood fit to the signal and background distributions. The signal is fitted with a Breit–Wigner function convoluted with the Gaussian detector resolution. In addition, reflections from the decays $D_1^+ \to D^{*0}\pi^+$ and $D_2^{*+} \to D^0\pi^+$ are taken into account in the fit to the $D_{s1}^+ \to D^{*0}K^+$ and $D_{s2}^{*+} \to D^0K^+$ distributions. This contribution is small due to the broad distribution of the reflection events and is determined from simulated events to be 4% (6%) of the $D_{s1}^+ \to D^{*0}K^+$ ($D_{s2}^{*+} \to D^0K^+$) signal events. The results of the fit to the ΔM_3 distributions are listed in Table 4. The systematic uncertainties on the measured mass differences are obtained by varying, in the fit, the assumed decay width and the detector resolution, as described in Section 5.1.

From the measured mass differences, the mass of the D_{s1}^+ and D_{s2}^{*+} can be calculated by adding the appropriate nominal mass (D^{*+}, D^{*0} or D^0) and calculating the weighted average in the case of the D_{s1}^+. The resulting masses are $m(D_{s1}^+) = 2535.3 \pm 0.7$ MeV/c^2 and $m(D_{s2}^{*+}) = 2568.6 \pm 3.2$ MeV/c^2. The measured masses are in good agreement with the world averages given in Table 1.

Table 5
Number of signal events in the c- and b-quark-enriched event sample

Decay channel	c-quark-enriched sample	b-quark-enriched sample
$D_{s1}^+ \to D^{*+}K^0$	$21.4 \pm 5.0_{\text{stat}} \pm 0.2_{\text{syst}}$	$15.1 \pm 5.3_{\text{stat}}{}^{+0.8}_{-1.7\text{syst}}$
$D_{s1}^+ \to D^{*0}K^+$	$32.2 \pm 9.3_{\text{stat}} \pm 1.3_{\text{syst}}$	$15.4 \pm 7.8_{\text{stat}} \pm 1.8_{\text{syst}}$
$D_{s2}^{*+} \to D^0K^+$	$30.7 \pm 14.1_{\text{stat}}{}^{+2.6}_{-5.2\text{syst}}$	$14.6 \pm 14.2_{\text{stat}}{}^{+2.6}_{-4.9\text{syst}}$

3.3. Measurement of D_s^{**} *decays in the* c- *and* b-*quark-enriched sample*

The measured mass-difference distributions for the c- and b-quark-enriched samples are shown in Figs. 4 and 5. The D_{s1} and D_{s2}^* mesons are reconstructed as described in the previous sections. The numbers of signal events are determined with an unbinned log-likelihood fit to the data as described in the previous section, with the exception that the mass differences are fixed using the D_{s1} and D_{s2}^* masses given in Table 1. The results are given in Table 5.

4. Reconstruction efficiencies

To determine the production rates in hadronic events, the reconstruction efficiencies are taken from the simulation. The efficiencies are calculated separately for D_s^{**} mesons produced in charm fragmentation, b-hadron decays and from gluon splitting.

In the flavour-independent selection the reconstruction efficiencies for D_s^{**} mesons produced in charm fragmentation and in b-hadron decays are approximately the same. The efficiency for D_s^{**} mesons from gluon splitting is lower due to their softer energy spectrum. The mean efficiencies are calculated from the flavour-specific efficiencies under the assumption that D_s^{**} mesons are produced in equal amounts in charm fragmentation and in b-hadron decays. The fraction of D_s^{**} mesons produced in gluon splitting is taken from the simulation, with the rate of gluons splitting into $c\bar{c}$ pairs reweighted to the measured value of $f(g \to c\bar{c}) = 0.0296 \pm 0.0038$ [15], and found to be about 6%. The average efficiency is calculated as $\epsilon_m = 0.47\epsilon_c + 0.47\epsilon_b + 0.06\epsilon_g$. The calculated mean efficiencies are given in Table 6.

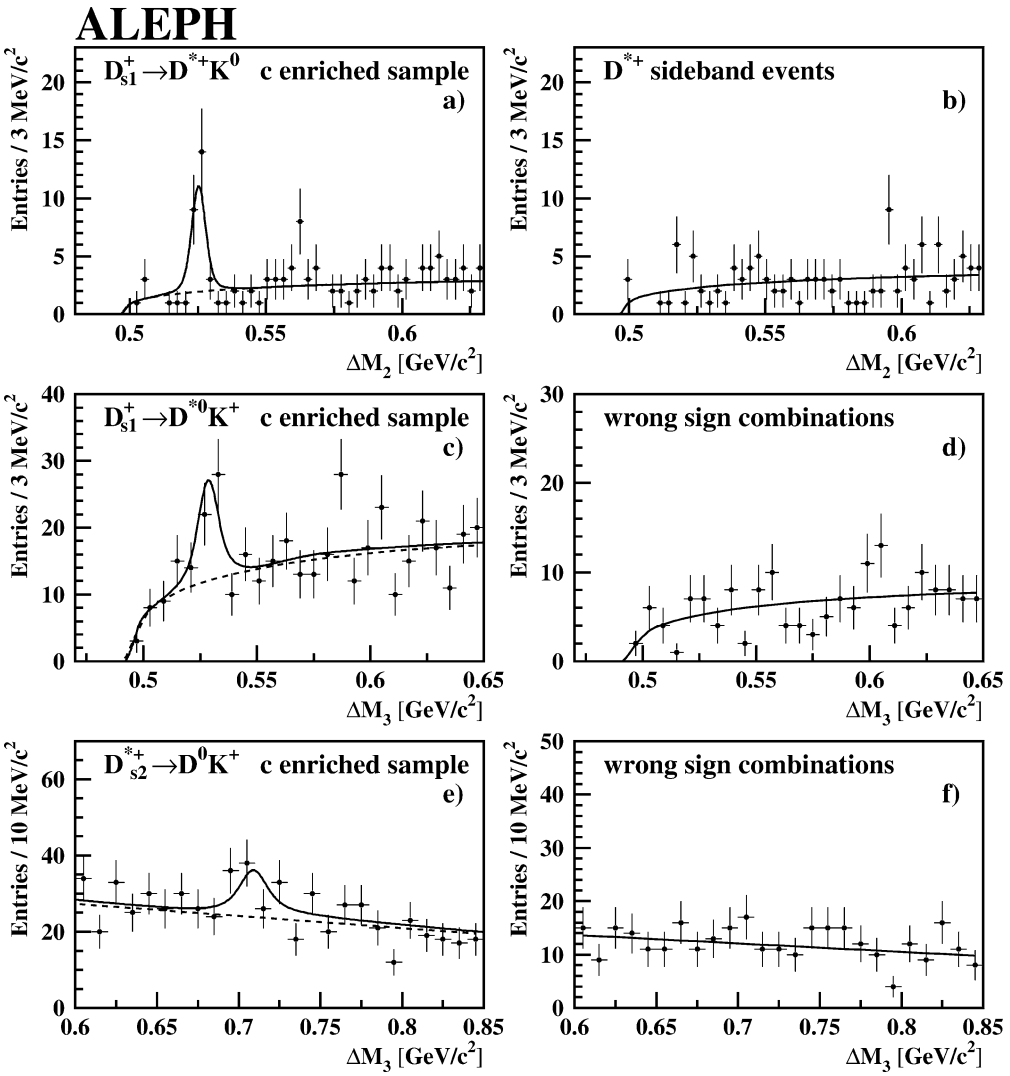

Fig. 4. Reconstructed mass-difference distribution for the c-quark-enriched event sample. The full curve is the result of an unbinned log-likelihood fit and the dashed curve represents the combinatorial background.

Table 6
Mean reconstruction efficiencies of the decays $D_{s1}^{+} \to D^{*+}K^{0}$, $D_{s1}^{+} \to D^{*0}K^{+}$ and $D_{s2}^{*+} \to D^{0}K^{+}$

Decay channel	Mean efficiency
$D_{s1}^{+} \to D^{*+}K^{0}$ ($D^{0} \to K^{-}\pi^{+}$)	$(16.46 \pm 0.41)\%$
$D_{s1}^{+} \to D^{*+}K^{0}$ ($D^{0} \to \overline{K}^{0}\pi^{+}\pi^{-}$)	$(11.70 \pm 0.51)\%$
$D_{s1}^{+} \to D^{*+}K^{0}$ ($D^{0} \to K^{-}\pi^{+}\pi^{-}\pi^{+}$)	$(9.17 \pm 0.22)\%$
$D_{s1}^{+} \to D^{*+}K^{0}$ ($D^{0} \to K^{-}\pi^{+}\pi^{0}$)	$(2.99 \pm 0.11)\%$
$D_{s1}^{+} \to D^{*0}K^{+}$	$(11.00 \pm 0.14)\%$
$D_{s2}^{*+} \to D^{0}K^{+}$	$(10.73 \pm 0.18)\%$

The reconstruction efficiencies in the c- and the b-quark-enriched event samples for the different D_s^{**} decays are listed in Table 7.

5. Production rates

The production rates are calculated from the observed number of events, the total number of hadronic Z decays ($N_{\mathrm{evt}} = 4\,151\,890$), the known branching ra-

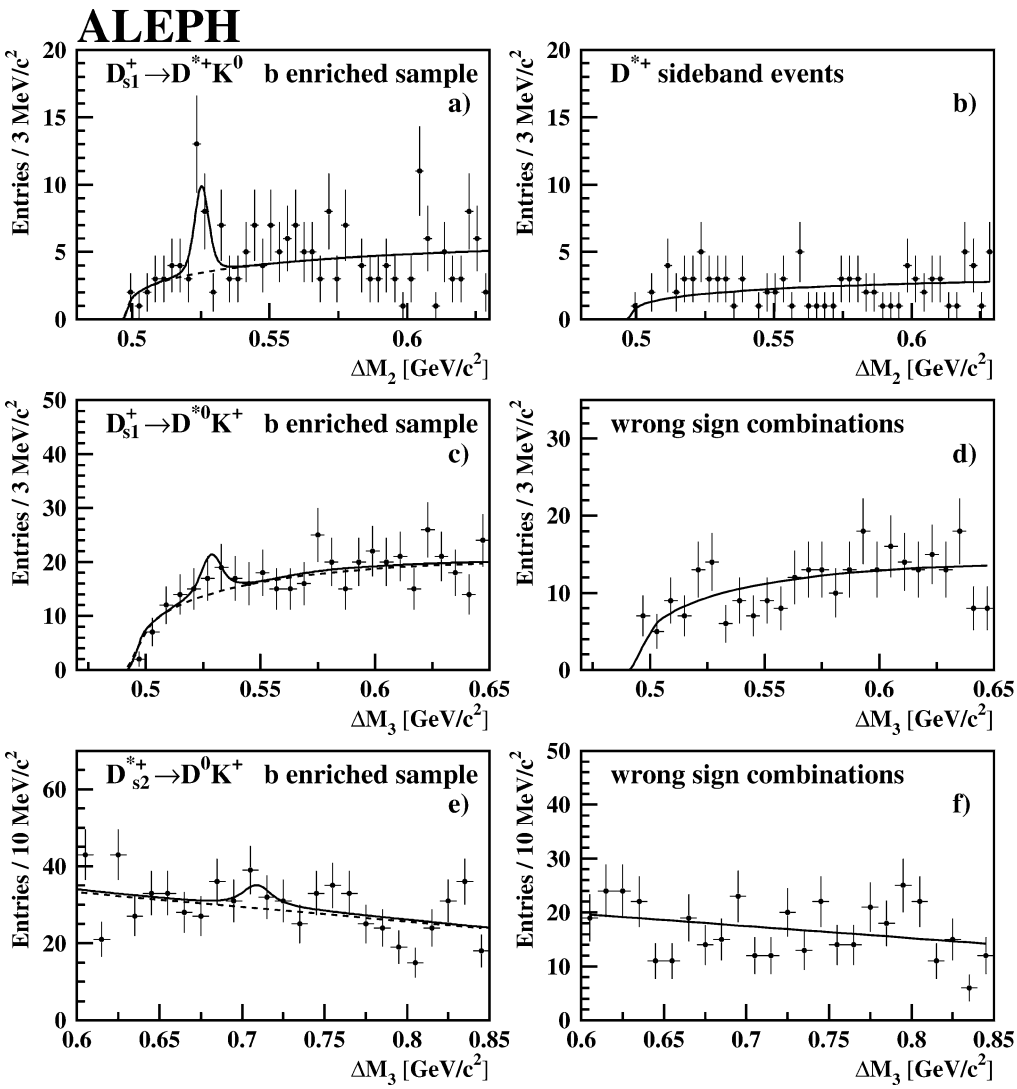

Fig. 5. Reconstructed mass-difference distribution for the b-quark-enriched event sample. The full curve is the result of an unbinned log-likelihood fit to the data and the dashed curve represents the combinatorial background.

Table 7
Reconstruction efficiencies for the decays $D_{s1}^{+} \to D^{*+}K^{0}$, $D_{s1}^{+} \to D^{*0}K^{+}$ and $D_{s2}^{*+} \to D^{0}K^{+}$ in the c- and b-quark-enriched event samples. For the decay $D_{s1}^{+} \to D^{*+}K^{0}$ the reconstruction efficiencies are branching-ratio-weighted sums of the four different D^{0} decay modes. The low efficiency for $b \to D_s^{**}$ ($c \to D_s^{**}$) in the c-quark (b-quark) enriched sample reflects the contamination of approximately 10–15% of the other flavour.

	c-quark-enriched		b-quark-enriched	
Decay channel	$c \to D_s^{**}$	$b \to D_s^{**}$	$c \to D_s^{**}$	$b \to D_s^{**}$
$D_{s1}^{+} \to D^{*+}K^{0}$	$(5.87 \pm 0.30)\%$	$(0.88 \pm 0.14)\%$	$(0.34 \pm 0.04)\%$	$(4.08 \pm 0.20)\%$
$D_{s1}^{+} \to D^{*0}K^{+}$	$(9.14 \pm 0.22)\%$	$(1.40 \pm 0.06)\%$	$(0.70 \pm 0.06)\%$	$(7.81 \pm 0.15)\%$
$D_{s2}^{*+} \to D^{0}K^{+}$	$(9.99 \pm 0.18)\%$	$(1.36 \pm 0.08)\%$	$(0.59 \pm 0.05)\%$	$(7.34 \pm 0.17)\%$

tios and the reconstruction efficiencies

$$f\left(\mathrm{Z}\to \mathrm{D}_{\mathrm{s1}}^{\pm}\right)\mathrm{Br}\left(\mathrm{D}_{\mathrm{s1}}^{+}\to \mathrm{D}^{*+}\mathrm{K}^{0}\right) = \frac{2n_1}{N_{\mathrm{evt}}\epsilon_1\,\mathrm{Br}(\mathrm{D}^{*+}\to \mathrm{D}^{0}\pi^{+})\,\mathrm{Br}(\mathrm{K}_{\mathrm{S}}^{0}\to \pi^{+}\pi^{-})}, \quad (1)$$

$$f\left(\mathrm{Z}\to \mathrm{D}_{\mathrm{s1}}^{\pm}\right)\mathrm{Br}\left(\mathrm{D}_{\mathrm{s1}}^{+}\to \mathrm{D}^{*0}\mathrm{K}^{+}\right) = \frac{n_2}{N_{\mathrm{evt}}\epsilon_2\,\mathrm{Br}(\mathrm{D}^{0}\to \mathrm{K}^{-}\pi^{+})}, \quad (2)$$

$$f\left(\mathrm{Z}\to \mathrm{D}_{\mathrm{s2}}^{*\pm}\right)\mathrm{Br}\left(\mathrm{D}_{\mathrm{s2}}^{*+}\to \mathrm{D}^{0}\mathrm{K}^{+}\right) = \frac{n_3}{N_{\mathrm{evt}}\epsilon_3\,\mathrm{Br}(\mathrm{D}^{0}\to \mathrm{K}^{-}\pi^{+})}, \quad (3)$$

where n_1, n_2 and n_3 denote the number of reconstructed events in the three considered $\mathrm{D}_{\mathrm{s}}^{**}$ channels and ϵ_1, ϵ_2 and ϵ_3 the corresponding branching-ratio-weighted sums of the reconstruction efficiencies. The branching ratios of the D^{*+}, $\mathrm{K}_{\mathrm{S}}^{0}$, D^{0}, and those of all subsequent decays, are taken from [7].

In the case of the c- and b-quark-enriched samples, the rate is calculated per event hemisphere and not per Z-decay. In this case the number of hadronic events are multiplied by the partial width $\mathrm{R_c}$ and $\mathrm{R_b}$, for which the Standard Model values $\mathrm{R_c} = 17.2\%$ and $\mathrm{R_b} = 21.6\%$ are used. The average number of $\mathrm{D}_{\mathrm{s}}^{**}$ expected from gluon splitting (1–2%) is subtracted from the number of events observed. Since the enriched samples are not pure, but have a contamination of roughly 10% from other quark flavours, the production rates are determined simultaneously for the c- and b-quark-enriched samples.

5.1. Systematic errors

The main contribution to the systematic error originates from the uncertainty on the parameters held fixed in the fit to the mass distributions of the $\mathrm{D}_{\mathrm{s1}}^{+}$ and $\mathrm{D}_{\mathrm{s2}}^{*+}$ candidates. In all fits the natural decay widths ($\Gamma(\mathrm{D}_{\mathrm{s1}}^{\pm}) = 1.5$ MeV and $\Gamma(\mathrm{D}_{\mathrm{s2}}^{*\pm}) = 15$ MeV) and the detector resolution are fixed. In order to determine the systematic error, the decay width of the $\mathrm{D}_{\mathrm{s1}}^{\pm}$ ($\mathrm{D}_{\mathrm{s2}}^{*\pm}$) is varied between 1 and 2 MeV (10 and 20 MeV). An uncertainty of $\pm 10\%$ is assumed for the detector resolution determined from the simulation. In the case of the c- and b-quark-enriched samples, the central values of the $\mathrm{D}_{\mathrm{s1}}^{+}$ and $\mathrm{D}_{\mathrm{s2}}^{*+}$ masses are fixed to the world averages [7] and are varied by ± 0.6 MeV/c^2 for the $\mathrm{D}_{\mathrm{s1}}^{+}$ and by ± 2 MeV/c^2 for the $\mathrm{D}_{\mathrm{s2}}^{*+}$. Each parameter is varied independently and the change in the number of signal events is taken as the systematic error from that particular source. The total systematic error listed in Tables 4 and 5 is given by the quadratic sum of all the above contributions.

The rate of gluons splitting to $\mathrm{c\bar{c}}$ pairs is varied within the experimental uncertainties. In addition, the selection efficiency for $\mathrm{D}_{\mathrm{s}}^{**}$ mesons originating from this source is varied by 50% to account for the modeling of the $\mathrm{g}\to \mathrm{c\bar{c}}$ process. An error of 20% is assumed on the equality of the $\mathrm{D}_{\mathrm{s}}^{**}$ production in c- and b-events, which is used in the calculation of the average efficiency (see Section 4). The resulting error on the production rate is 1%.

The fraction of reflection events from D^{**} decays is taken from the simulation. The obtained ratio between reflection and signal events is varied by 50% and the corresponding change in the number of signal events taken as the systematic error.

In the simulation the parameters of the Peterson fragmentation function are reweighted to reproduce the measured values of the mean scaled energy x_E of c- and b-hadrons: $x_E(\mathrm{c}) = 0.484 \pm 0.008$ and $x_E(\mathrm{b}) = 0.702 \pm 0.008$ [14], respectively. The reweighted samples are used to determine the reconstruction efficiencies and the errors on the fragmentation parameters are propagated as well.

The dE/dx selection efficiency determined from the simulation is tested by reconstructing $\mathrm{D}^{*+}\to (\mathrm{K}^{-}\pi^{+})\pi^{+}$ decays without using the dE/dx information of the K^{-}. By applying subsequently the dE/dx cut used in the analysis, the efficiency of this cut can be determined in data and the simulation. The difference between data and the simulation is $(-3.8 \pm 2.9)\%$. The reconstruction efficiencies of the appropriate decay channels are corrected for the observed offset and the uncertainty is taken into account as a systematic error.

Finally the errors of the reconstruction efficiency due to the finite Monte Carlo statistics and the uncertainty on the used branching ratios are taken into account.

The total systematic error is calculated by adding the different contributions in quadrature. The list of the systematic errors is given in Table 8. The systematic errors of the two $\mathrm{D_{s1}}$-modes have been assumed to be 100% correlated.

Table 8
Systematic error contributions in %

Error source	Flavour independent	c-enriched	b-enriched
	Systematic errors in the decay $D_{s1}^{+} \to D^{*+}K^{0}$		
Mass, decay width and resolution	$+8\ -9$	±1	$+5\ -11$
$x_E(c)$, $x_E(b)$ variation	±1	±1	±1
Kaon dE/dx selection	±3	±3	±3
D_s^{**} source (gluon, c and b)	±3	±1	±1
Monte Carlo statistics	±3	±3	±4
D^0 branching ratios	±5	±5	±5
Total	$+11\ -12$	±7	$+9\ -13$
	Systematic errors in the decay $D_{s1}^{+} \to D^{*0}K^{+}$		
Mass, decay width and resolution	±8	±4	±12
$x_E(c)$, $x_E(b)$ variation	±1	±1	±2
Kaon dE/dx selection	±3	±3	±3
D^{**} reflections	±2	±4	$+3\ -2$
D_s^{**} source (gluon, c and b)	±3	±1	±1
Monte Calo statistics	±1	±1	±1
D^0 branching ratio	±2	±2	±2
Total	±10	±7	±13
	Systematic errors in the decay $D_{s2}^{*+} \to D^{0}K^{+}$		
Mass, decay width and resolution	$+7\ -15$	$+9\ -17$	$+18\ -34$
$x_E(c)$, $x_E(b)$ variation	±1	±1	±2
Kaon dE/dx selection	±3	±3	±3
D^{**} reflections	±3	±3	±14
D_s^{**}source (gluon, c and b)	±3	±1	±1
Monte Carlo statistics	±1	±1	±1
D^0 branching ratio	±2	±2	±2
Total	$+9\ -16$	$+10\ -18$	$+23\ -37$

5.2. Results

From the measured numbers of produced $D_{s1}^{\pm}$ and $D_{s2}^{*\pm}$ mesons and the reconstruction efficiencies, the production rates in the decay channels $D_{s1}^{+} \to D^{*+}K^{0}$, $D_{s1}^{+} \to D^{*0}K^{+}$ and $D_{s2}^{*+} \to D^{0}K^{+}$ in hadronic events are

$$f\left(Z \to D_{s1}^{\pm}\right) \mathrm{Br}\left(D_{s1}^{+} \to D^{*+}K^{0}\right) = (0.22 \pm 0.05_{\mathrm{stat}} \pm 0.03_{\mathrm{syst}})\%,$$

$$f\left(Z \to D_{s1}^{\pm}\right) \mathrm{Br}\left(D_{s1}^{+} \to D^{*0}K^{+}\right) = (0.29 \pm 0.08_{\mathrm{stat}} \pm 0.03_{\mathrm{syst}})\%,$$

$$f\left(Z \to D_{s2}^{*\pm}\right) \mathrm{Br}\left(D_{s2}^{*+} \to D^{0}K^{+}\right) = \left(0.37 \pm 0.13_{\mathrm{stat}}{}^{+0.03}_{-0.06\,\mathrm{syst}}\right)\%.$$

The production rates in the c-quark-enriched sample are

$$f\left(c \to D_{s1}^{\pm}\right) \mathrm{Br}\left(D_{s1}^{+} \to D^{*+}K^{0}\right) = (0.35 \pm 0.10_{\mathrm{stat}} \pm 0.03_{\mathrm{syst}})\%,$$

$$f\left(c \to D_{s1}^{\pm}\right) \mathrm{Br}\left(D_{s1}^{+} \to D^{*0}K^{+}\right) = (0.59 \pm 0.19_{\mathrm{stat}} \pm 0.04_{\mathrm{syst}})\%,$$

$$f\left(c \to D_{s2}^{*\pm}\right) \mathrm{Br}\left(D_{s2}^{*+} \to D^{0}K^{+}\right) = \left(0.51 \pm 0.27_{\mathrm{stat}}{}^{+0.05}_{-0.09\,\mathrm{syst}}\right)\%.$$

The production rates in the b-quark-enriched sample are

$$f\left(b \to D_{s1}^{\pm}\right) \mathrm{Br}\left(D_{s1}^{+} \to D^{*+}K^{0}\right) = \left(0.30 \pm 0.12_{\mathrm{stat}}{}^{+0.03}_{-0.04\,\mathrm{syst}}\right)\%,$$

$$f\left(b \to D_{s1}^{\pm}\right) \mathrm{Br}\left(D_{s1}^{+} \to D^{*0}K^{+}\right) = (0.24 \pm 0.15_{\mathrm{stat}} \pm 0.03_{\mathrm{syst}})\%,$$

$$f\left(b \to D_{s2}^{*\pm}\right) \mathrm{Br}\left(D_{s2}^{*+} \to D^{0}K^{+}\right) = \left(0.25 \pm 0.29_{\mathrm{stat}}{}^{+0.06}_{-0.09\,\mathrm{syst}}\right)\%.$$

The production rate of $D_{s2}^{*\pm}$ mesons in b-decays has a significance of less than one sigma, therefore a 95% confidence limit is calculated by renormalizing the probability for the allowed region of the production rate and taking into account the measured central value:

$$f(b \to D_{s2}^{*\pm}) \,\mathrm{Br}(D_{s2}^{*+} \to D^0 K^+) < 0.77\% \text{ at 95\% CL.}$$

Assuming that the decay width of the D_{s1}^+ is saturated by the two measured decays and that the branching ratio $\mathrm{Br}(D_{s2}^{*+} \to D^0 K^+)$ is 45%, which follows from the assumption that $\mathrm{Br}(D_{s2}^{*+} \to DK) = 90\%$ with 10% branching ratio into D^*K [8], the total production rates in hadronic events are found to be

$$f(Z \to D_{s1}^{\pm}) = (0.52 \pm 0.09_{\mathrm{stat}} \pm 0.06_{\mathrm{syst}})\%,$$
$$f(Z \to D_{s2}^{*\pm}) = \left(0.83 \pm 0.29_{\mathrm{stat}}{}^{+0.07}_{-0.13\,\mathrm{syst}}\right)\%.$$

The production rates from c-quarks ($c \to D_s^{**}$) are

$$f(c \to D_{s1}^{\pm}) = (0.94 \pm 0.22_{\mathrm{stat}} \pm 0.07_{\mathrm{syst}})\%,$$
$$f(c \to D_{s2}^{*\pm}) = \left(1.14 \pm 0.59_{\mathrm{stat}}{}^{+0.11}_{-0.20\,\mathrm{syst}}\right)\%.$$

The production rates from b-quarks ($b \to D_s^{**}$) are

$$f(b \to D_{s1}^{\pm}) = \left(0.55 \pm 0.19_{\mathrm{stat}}{}^{+0.06}_{-0.07\,\mathrm{syst}}\right)\%,$$
$$f(b \to D_{s2}^{*\pm}) = \left(0.57 \pm 0.63_{\mathrm{stat}}{}^{+0.13}_{-0.20\,\mathrm{syst}}\right)\%.$$

The production rate of $D_{s2}^{*\pm}$ mesons in b-decays has a significance of less than one sigma and the corresponding upper limit is

$$f(b \to D_{s2}^{*\pm}) < 1.70\% \text{ at 95\% CL.}$$

6. Conclusions

The production rates of the D_s^{**} mesons D_{s1}^+ and D_{s2}^{*+} have been measured by reconstructing the decays $D_{s1}^+ \to D^{*+}K^0$, $D_{s1}^+ \to D^{*0}K^+$ and $D_{s2}^{*+} \to D^0K^+$.

In the two measured D_{s1}^+ decay modes an enhancement of the $D^{*0}K^+$ final state is expected due to the higher Q-value of the decay, since isospin invariance requires the matrix elements of the two decays to be the same. The expected ratio of the two branching ratios is given by [8]

$$\frac{\mathrm{Br}(D_{s1}^+ \to D^{*0}K^+)}{\mathrm{Br}(D_{s1}^+ \to D^{*+}K^0)} = \left(\frac{q(K^+)}{q(K^0)}\right)^{2L+1} \approx 1.77,$$

where $q(K^+)$ ($q(K^0)$) is the momentum of the K^+ (K^0) in the rest frame of the D_{s1}^+ and $L = 2$ for a pure D-wave decay.

The measured ratio of the two production rates is

$$\frac{\mathrm{Br}(D_{s1}^+ \to D^{*0}K^+)}{\mathrm{Br}(D_{s1}^+ \to D^{*+}K^0)} = 1.32 \pm 0.47_{\mathrm{stat}} \pm 0.23_{\mathrm{syst}}.$$

The smaller value compared with the expectation could be due to an admixture of a S-wave decay from one of the broad D_s^{**} states (see Table 1). However, no significant discrepancy with the expected production rate ratio for a pure D-wave decay is observed.

Acknowledgements

It is a pleasure to thank our colleagues in the accelerator divisions of CERN for the excellent performance of LEP. Thanks are also due to the technical personnel of the collaborating institutions for their support in constructing and maintaining the ALEPH experiment. Those of us not from member states wish to thank CERN for its hospitality.

References

[1] N. Isgur, M.B. Wise, Phys. Rev. Lett. 66 (1991) 1130.
[2] J.L. Rosner, Comments Nucl. Part. Phys. 16 (1986) 109.
[3] ARGUS Collaboration, Phys. Lett. B 297 (1992) 425.
[4] CLEO Collaboration, Phys. Lett. B 303 (1993) 377.
[5] CLEO Collaboration, Phys. Rev. Lett. 72 (1994) 1972.
[6] OPAL Collaboration, Z. Phys C 76 (1997) 425.
[7] Particle Data Group, Eur. Phys. J. C 15 (2000).
[8] S. Godfrey, R. Kokoski, Phys. Rev. D 43 (1991) 1679.
[9] ALEPH Collaboration, Nucl. Instrum. Methods A 294 (1990) 121;
B. Mours et al., Nucl. Instrum. Methods A 379 (1996) 101.
[10] ALEPH Collaboration, Nucl. Instrum. Methods A 360 (1995) 481.
[11] ALEPH Collaboration, Z. Phys. C 53 (1992) 1.
[12] ALEPH Collaboration, Z. Phys. C 64 (1994) 361.
[13] ALEPH Collaboration, Phys. Lett. B 313 (1993) 535.
[14] ALEPH, CDF, DELPHI, L3, OPAL, SLD Collaborations, Combined results on b-hadron production rates, lifetimes, oscillations and semileptonic decays, CERN-EP-2000-096.
[15] ALEPH, CDF, DELPHI, L3, OPAL, SLD Collaborations, Precision electroweak measurements on the Z resonance, Phys. Rep., in preparation.